

Dissolved-recrystallized zircon from mariupolite in the Mariupol Massif, Priazovje (SE Ukraine)

MAGDALENA DUMAŃSKA-SŁOWIK¹, MAGDALENA SIKORSKA² AND WIESŁAW HEFLIK¹

¹*Department of Mineralogy, Petrography and Geochemistry, Faculty of Geology, Geophysics and Environmental Protection, AGH – University of Science and Technology, Kraków PL-30-059, Mickiewicza 30, Poland, E-mail: dumanska@uci.agh.edu.pl*

²*Polish Geological Institute-National Research Institute, 4 Rakowiecka St., PL-00-975 Warsaw, Poland.*

ABSTRACT:

Dumańska-Słowik, M., Sikorska, M. and Heflik, W. 2011. Dissolved-recrystallized zircon from mariupolite in the Mariupol Massif, Priazovje (SE Ukraine). *Acta Geologica Polonica*, **61** (3), 277–288. Warszawa.

Zircon in *mariupolite* from the alkaline Mariupol Massif has a relatively simple, monotonous composition with only some variation in its REE₂O₃ and ThO₂ content, i.e., 0.00–1.55 and 0.00–0.34 wt. %, respectively. It contains numerous inclusions such as albite, lepidomelane, aegirine, K-feldspars, pyrochlore, paristite and bastnäsite-(Ce). The crystallization of the inclusions (except for REE-bearing carbonates) was contemporaneous with the formation of the zircon crystals. These inclusions were enclosed by faster growing zircons. The SEM-CL images of the zircon are typical of crystals with signs of local thermal recrystallization, i.e., primary oscillatory zoning along the grain margins and secondary irregular patchy zoning in the interior. Its complex internal texture most probably formed as a result of a coupled dissolution-recrystallization process during the late magmatic or post-magmatic stage of the cooling of the host rocks. The abundant micropores could have originated as a result of leaching of the zircon. The recrystallization process definitely disturbed the concentric oscillatory zoning pattern characteristic of magmatic zircon.

Key words: Zircon; Mariupolite; REE; Dissolution and recrystallization.

INTRODUCTION

Zircon is a ubiquitous accessory mineral present in many types of igneous, metamorphic and sedimentary rocks and is particularly common in alkali plutonic rocks. It is chemically resistant and refractory and it can endure both weathering and transport processes as well as high temperature metamorphism and anatexis (Hinton and Upton 1991; Belousova *et al.* 2002). However, zircon is not immutable; some geological events that it undergoes leave their imprints in the form of growth or degradation (e.g., partial dissolution, metamictization, mechanical breakage) of crystals (Hanchar and Miller 1993).

Zircon generally occurs as small, early-formed grains, but may also form large well-developed crystals in granites, pegmatites and, most commonly, nepheline syenite (Deer *et al.* 1992)

A number of studies have been carried out on zircon chemistry, structure and textures, on the chemical and structural alteration of the crystals originating from different geological environments, and on the zircon U-Pb geochronology of granitic and high-grade metamorphic rocks (e.g. Murali *et al.* 1983; Rubin *et al.* 1989; Hinton and Upton 1991; Vavra *et al.* 1999; Rubatto and Gebauer 2000; Geisler *et al.* 2003; Hoskin 2005; Gagnevin *et al.* 2009; and many others). Some studies were focused on zircon luminescence, but this issue still remains poorly understood (e.g., Marshall 1988; Hanchar and Miller 1993; Belousova *et al.* 1998; Gotze 2000; Kempe *et al.* 2000; Gorobets and Rogojine 2002; Corfu *et al.* 2003; Nasdala *et al.* 2003; Gaft *et al.* 2005). The CL of zircon is generally caused by intrinsic (lattice defects) or extrinsic defect centres (e.g., trace elements such as REE). The luminescence in natural zir-

con is dominated by narrow emission lines ascribed to Dy^{3+} and a broad emission arising from radiation-induced centres. The weaker luminescence lines of some REE elements are obscured by the stronger luminescence of others and not all the REE can be identified then (Gaft *et al.* 2005). Dy^{3+} is the dominant activator element in all zircons with a blue CL colour, whereas yellow CL is associated with the radioactive decay of trace amounts of uranium (Nicholas 1967). Most likely there are a number of other centres responsible for the yellow CL (Gorobets and Rogojine 2002).

This paper focuses on texture and the trace-element geochemistry of zircon originating from mariupolite, a leucocratic variety of nepheline syenite from the Mariupol massif in SE Ukraine. The material was analysed using SEM-EDS, EPMA and CL methods. The trace element concentration necessary for luminescence activation can be very low, often below the detection limit of an electron microprobe. Therefore CL is much more sensitive as a geochemical tool than EPMA. Based on the internal texture of the crystals and the distribution of trace elements, the authors tried to reconstruct the growth history of the zircon.

GEOLOGICAL SETTING

The alkaline Mariupol (Oktyabrski) massif, situated in a north-western part of the eastern Pripetian region, approximately 3 km south of Volnovakha and 50 km south-east of Donetsk (south-eastern Ukraine), is a unique province of alkaline magmatism of Proterozoic age *ca.* 1.8 Ga (Volkova 2000, 2001). It covers an area of 34 km² (Krividik *et al.* 2007). The Mariupol massif is oval-shaped, with a N–S elongation. It has a concentric structure: in the centre there are pulaskites, i.e., nepheline-bearing alkali feldspar syenites with variable proportions of dark minerals such as Na-bearing pyroxenes and amphiboles, fayalite and biotite, which are surrounded by foyaites, i.e., nepheline syenites composed mainly of K-feldspar and nepheline. The latter are in turn enclosed by syenites. *Mariupolites*, the microcline-nepheline syenites, forming veins of various thickness, occur in the periphery of this alkaline complex (Text-fig. 1). Ultramafic and mafic rocks (peridotites, pyroxenites and gabbros), probably formed at the early beginning of differentiation of typical mafic magma, occur in the outer ring of the massif.

The genesis of this massif has been under a debate for a long time. Tichonienkova *et al.* (1967) believed that the rocks of the Mariupol massif were formed as a result of post-magmatic and metasomatic alteration processes. The presence of *fenites*, high temperature

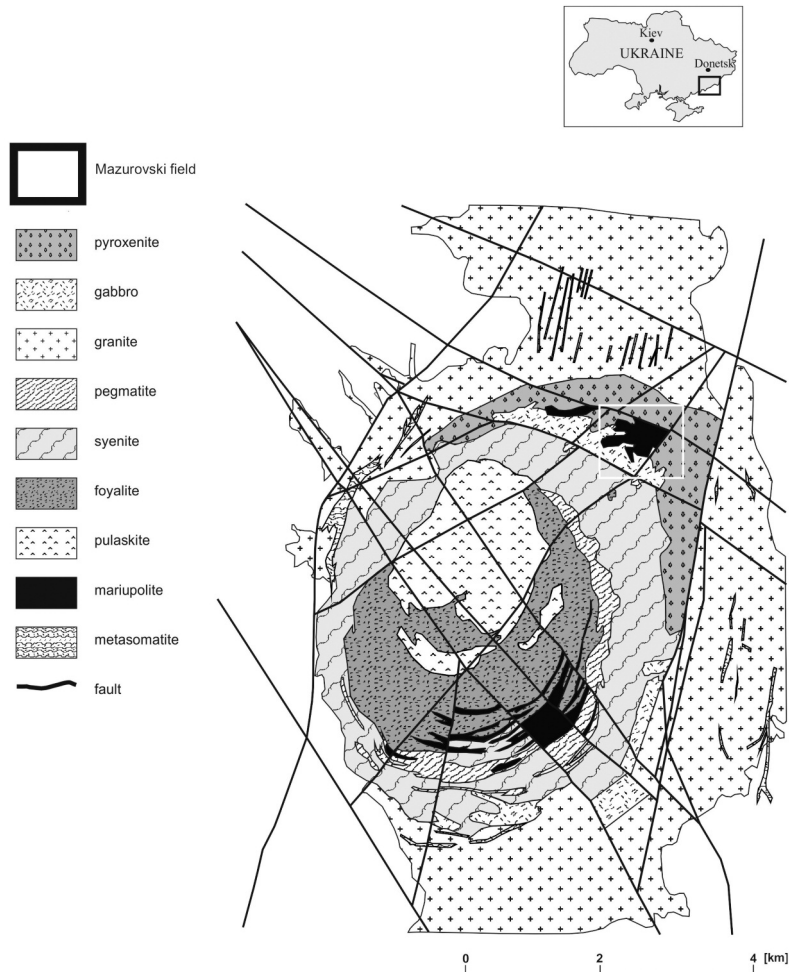
metasomatic rocks composed mainly of alkali feldspars, nepheline, Na-bearing pyroxenes and amphiboles, with subordinate phlogopite, magnetite and ilmenite, within the alkaline massif supported this thesis. Donskoy (1982) and Solodov (1985) suggested that a majority of the rocks crystallized due to differentiation of magma with the composition of nepheline syenite. However, they also agreed that metasomatic activity affecting the rocks was responsible for significant concentration of rare metals, such as the Nb and Zr deposits hosted by the rocks of this massif (Volkova 2001).

In the Mariupol massif, the agpaitic trend of magma differentiation was identified with the following rock genetic succession: subalkaline gabbro and its derivatives (pyroxenite and peridotite) – alkaline syenites – taramite foyaites – *mariupolites* – aegirine foyaites – eudialite-bearing phonolites (Krividik *et al.* 2007). The development of the agpaitic trend was associated with an increase in the trace elements Zr, Nb, Y, REE, Rb, and a decrease in Sr, Ba, P and Ti (Krividik and Tkachuk 1998). Nevertheless, agpaitic rocks are generally scarce in this massif.

Mariupolites (Morozewicz 1902, 1929) cover a small area (*ca.* 5–10%) of the whole massif. They are intermediate between the miaskitic and agpaitic types (Sharygin *et al.* 2009) and represent rare aegirine-nepheline-albite rocks, which contain also sodalite, cancrinite and lepidomelane. Zircon, pyrochlore, britholite and subordinate magnetite, hematite, ilmenite and rutile occur as accessory components.

Mariupolite petrography

Mariupolite has a fine- to medium crystalline fabric and contains albite (~61 vol. %), nepheline (~23 vol. %), K-feldspar (~11 vol. %), aegirine (2.5 vol. %), zircon (1.5 vol. %), lepidomelane (0.5 vol. %), pyrochlore (0.3 vol. %), fluorite, sodalite, apatite and monazite (0.2 vol. %). Albite ($Ab_{94-92}An_{6-8}$) occurs as thin prismatic crystals with inconsistent multiple twinning. Nepheline usually forms large xenomorphic crystals. Similarly, potassium feldspars form large tabular crystals with well developed cleavages along (001) and (010). Some of these reveal a cross-hatched pattern, typical of microcline, while others exhibit a non-uniform, wavy light extinction characteristic of potassium feldspars changing from orthoclase into microcline. Aegirine forms stout prismatic crystals of varying size with a low $\alpha:z$ extinction angle (~0°). Most crystals show strong pleochroism: α = green, β = pale green, γ = pale yellow-green. Lepidomelane that forms well-preserved flakes occurs locally in the rock. Zircon is abundant in the form of euhedral crystals with a characteristic oscillatory zoning pattern. Euhedral crystals,



Text-fig. 1. A geological map of the Mariupol massif (SE Ukraine) (from Dumańska-Słowik *et al.* 2011)

which occasionally turn into a subhedral pyrochlore form, occur in the interstices between the albite crystals and exhibit a characteristic reaction rim built of Fe-bearing chlorite. Only a few of them show weak oscillatory zoning, very often with irregular lighter and darker patches and numerous microfractures.

ANALYTICAL METHODS

The backscattered electron observations and cathodoluminescence analyses were conducted at the Polish Geological Institute-National Research Institute in Warsaw. BSE analysis was performed on polished sections using a LEO 1430 scanning electron microscope with an EDS Oxford ISIS 300 detector. The system operated at 20 kV accelerating voltage, 50 μ A current, in a high-vacuum mode, i.e. $6 \times 10^{-5} - 7 \times 10^{-6}$ Torr.

The cathodoluminescence (CL) observations were conducted on polished thin sections using a Cambridge Image Technology CCL 8200 MK3 device

(cold cathode) linked to a Nikon Optiphot 2 polarising microscope. CL photos were taken using a Microflex UFX-DX camera. The scanning electron microscopy with cathodoluminescence (SEM-CL) analyses utilised a LEO 1430 scanning electron microscope with the CL-image system (ASK-CL VIS View) and CL spectrometer (ASK SEM-CL).

Electron microprobe analyses (EPMA) were carried out at the Inter-Institute Analytical Complex for Minerals and Synthetic Substances of Warsaw University with a Cameca SX-100 operating in a wavelength-dispersive (WDS) mode under the following conditions: excitation voltage 15 kV, beam current 50 nA. The following standards, analytical lines and crystals were used: Si – diopside ($K\alpha$, TAP), Hf – Hf-SPI ($M\alpha$, TAP), Yb – REE 3 ($L\alpha$, LIF), Er – REE 1 ($L\alpha$, LIF), Ti – rutile ($K\alpha$, LIF), Zr – zircon ED2 ($L\alpha$, PET), P – apatite ($K\alpha$, PET), Y – YAG ($L\alpha$, PET), Th – ThO₂ synt. ($M\beta$, PET), Ce – CeP₅O₁₄ ($L\alpha$, PET). The detection limits of EPMA analyses for the elements are presented in Table 1. Peak and background analytical times for Zr and Si were 20s

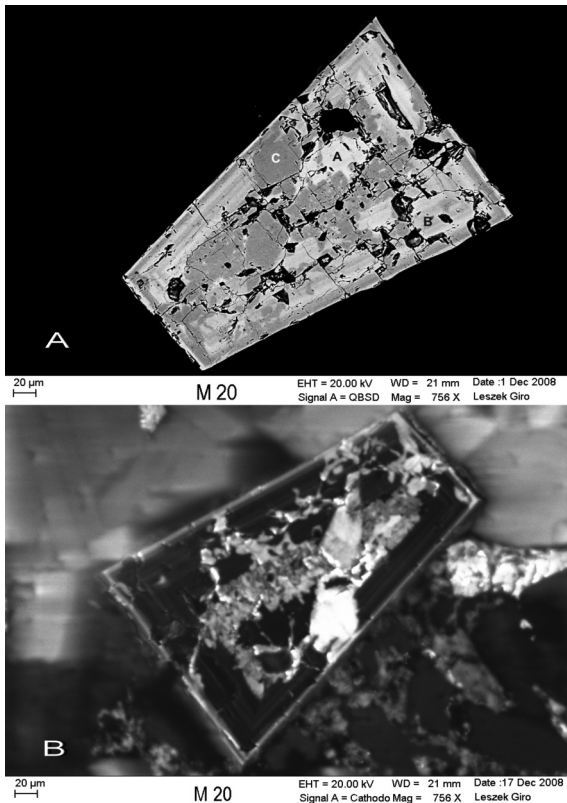
and 10+10, Ce, Ti and P - 30s and 15+15, Hf, Yb, Er - 40s and 20+20, U, Th and Y - 60s and 30+30 respectively. The data were corrected with the PAP procedure (Pouchou and Pichoir 1985) using an original software. The zircon formulae were calculated based on 4 oxygens.

Element	Detection limit (wt.%)
P	0.012
Si	0.006
Ti	0.027
Zr	0.070
Hf	0.023
Th	0.073
Y	0.016
Ce	0.038
Er	0.012
Yb	0.145

Table. 1. The EPMA detection limits for the elements occurring in zircon structure

RESULTS

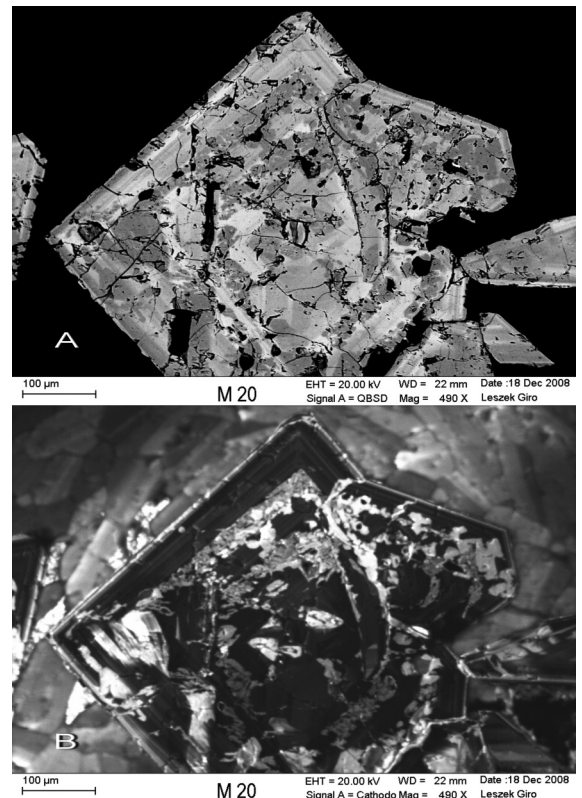
Zircon in *mariupolite* forms strongly fractured, tabular or prismatic crystals 0.1–2.0 mm in size. In transmitted light, BSE and CL images most crystals ex-



Text-fig. 2. Zircon crystal with irregular patchy zoning in its interior. A – BSE photo (A-bright patches, B- dark patches, C – darkest patches), B – SEM-CL image

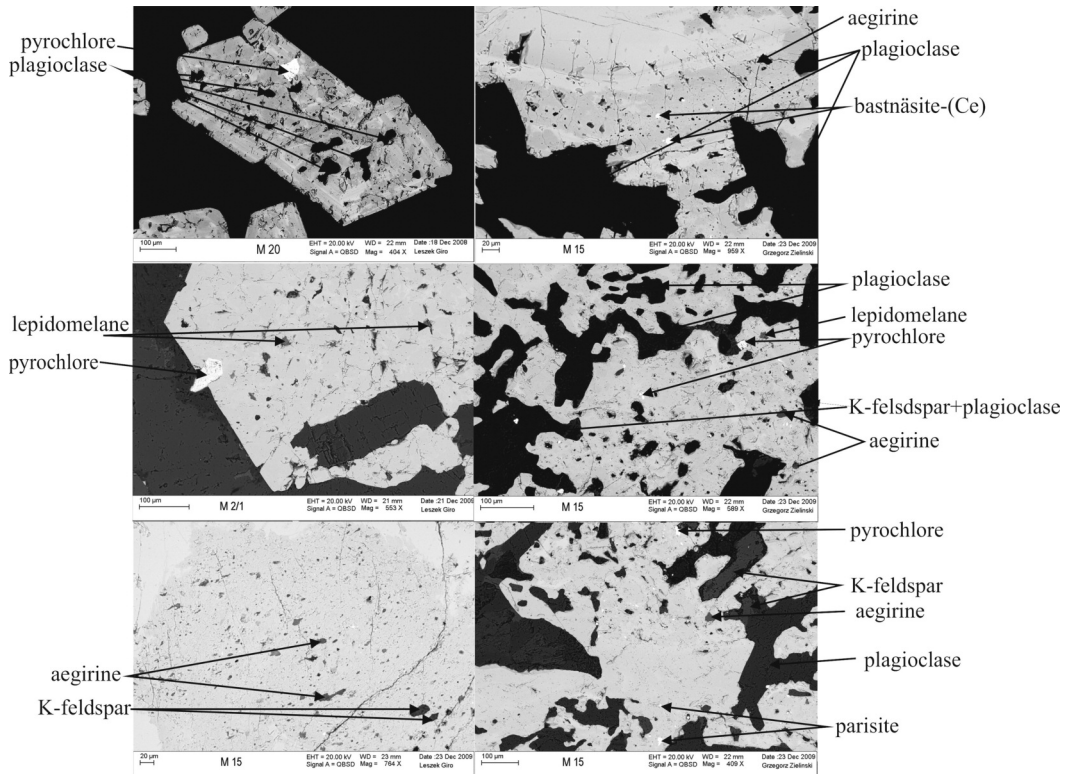
hibit distinct oscillatory zoning, with zones varying from 10 to 20 μm in width. In all large crystals light, darker and very dark patches (patchy zoning) are clearly observed (Text-fig. 2) in BSE images. Oscillatory zoning is especially well developed along the margins of the crystals, while an irregular patchy pattern appears mainly in the inner parts (Text-fig. 3). The patchy domains are regularly accompanied by numerous micropores which are filled with various inclusions, with plagioclase (albite) as the dominant phase, and lepidomelane, aegirine, and pyrochlore as the subordinate phases. Single paristite and bastnäsite-(Ce) crystals, which form tiny crystals ca. 10 μm in size, are also present in the zircon matrix (Text-fig. 4). The inclusion crystals are irregularly shaped and most of them have rounded edges (Text-fig. 5). Sometimes, their arrangement coincides well with (110) the cleavage plane of zircon.

The SEM-EDS investigations of the main rock-forming minerals of mariupolite and the same mineral phases appearing as the principal inclusions in the zircon, i.e., aegirine, lepidomelane, albite and K-feldspar, showed that the composition of their crystal structure differed somewhat (Table 2). Lepidomelane in the rock matrix contains more TiO_2 , MgO and MnO and no-

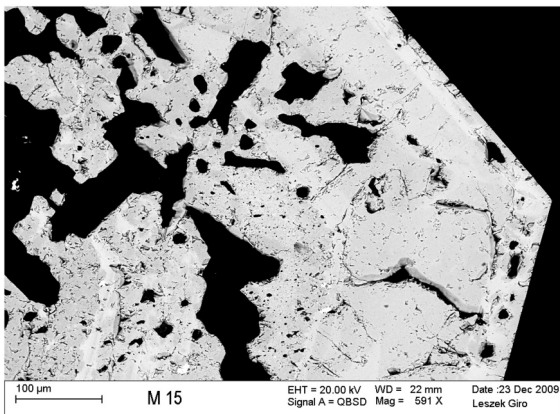


Text-fig. 3. Inter-growth of zircon crystals with oscillatory zoning along their margins and patchy zoning in their interiors. A – BSE photo, B – SEM-CL image

ZIRCON FROM MARIUPOLITE IN SE UKRAINE



Text-fig. 4. Inclusions in zircon crystals, BSE image



Text-fig. 5. A fractured region of zircon crystal with abundant micro-pores filled with various inclusions, BSE image

ticeably less Al_2O_3 , FeO and ZnO than the lepidomelane which occurs within zircon crystals (Text-fig. 6). Aegirine in mariupolite is slightly enriched in CaO and MnO, whereas aegirine from the zircon is completely devoid of these components (Text-fig. 7). The differences in composition of albite and K-feldspar from the rock matrix and zircon seem to be insignificant. The differences in the composition of aegirine and lepidomelane in the mariupolite matrix and in the zircon crystals are characteristic of chemical changes in the magma during its differentiation under conditions of falling temperature.

Zircon exhibits slight chemical variability; the distinct zones observed in BSE vary in chemical composition to some extent (Table 3). The light patches (i) are

Component (wt.%)	Lepidomelane in zircon	Lepidomelane in rock matrix	Aegirine in zircon	Aegirine in rock matrix	Albite in zircon	Albite in rock matrix	K-feldspar in zircon	K-feldspar in rock matrix
SiO_2	35.59	36.72	55.38	55.25	68.26	69.04	65.25	64.82
TiO_2	0.74	2.05	-	-	-	-	-	-
Al_2O_3	14.50	11.05	1.58	1.72	19.54	19.70	18.80	18.15
FeO	30.00	21.90	29.06	26.82	-	-	-	-
MnO	0.44	5.74	nd	0.80	-	-	-	-
MgO	1.97	7.27	-	-	-	-	-	-
CaO	-	-	nd	2.12	-	-	-	-
ZnO	3.60	0.78	-	-	-	-	-	-
Na_2O	2.00	1.28	14.69	13.87	11.27	10.77	0.25	0.95
K_2O	8.66	9.55	-	-	nd	nd	16.19	15.50
total	97.60	96.34	100.71	100.58	99.11	99.50	100.49	99.42

- not determined; nd – not detected

Table 2. Chemical composition of aegirine, lepidomelane, albite and K-feldspar occurring in zircon crystal and rock matrix, obtained with SEM-EDS method

enriched in REEs (0.009–0.023 apfu, 0.56–1.55 wt.% REE₂O₃). The sum of REEs clearly prevails over P (0.000–0.002 apfu, 0.00–0.07 wt.% P₂O₅). The hafnium content varies in a range from 0.007 to 0.008

apfu (0.74–0.90 wt.% HfO₂). The Th content is no more than 0.002 apfu (0.00–0.22 wt.%). The analytical totals are rather high 98.25–99.62 wt.%. The ZrO₂/HfO₂ ratios vary from 72 to 87. The dark patches

crystal region point no	bright patches										dark patches									
	3	14	15	19	22	23	29	32	34	35	40	1	5	8	9	11	12	13	16	
P ₂ O ₅	0.00	0.00	0.00	0.00	0.00	0.00	0.07	0.00	0.05	0.05	0.00	0.00	0.05	0.00	0.00	0.05	0.00	0.00	0.00	
SiO ₂	31.73	32.09	31.73	31.66	31.83	31.81	31.92	31.85	31.68	31.64	31.75	32.07	31.81	31.88	32.09	32.07	31.98	32.03	32.03	
TiO ₂	0.07	0.00	0.00	0.00	0.00	0.00	0.00	0.00	0.00	0.00	0.00	0.00	0.00	0.00	0.00	0.00	0.00	0.00	0.00	
ZrO ₂	65.08	65.88	65.61	64.93	64.93	64.51	66.03	65.13	64.65	64.31	64.93	66.84	66.23	65.46	66.36	67.31	66.40	66.26	66.70	
HfO ₂	0.90	0.83	0.84	0.87	0.90	0.85	0.86	0.79	0.74	0.90	0.84	0.74	0.80	0.78	0.96	1.04	0.84	0.88	0.85	
ThO ₂	0.19	0.14	0.17	0.15	0.16	0.20	0.00	0.22	0.17	0.19	0.22	0.11	0.00	0.24	0.00	0.00	0.00	0.00	0.00	
Y ₂ O ₃	1.00	0.61	0.63	0.93	0.91	1.07	0.50	0.56	0.94	0.74	0.61	0.39	0.66	0.86	0.46	0.05	0.42	0.25	0.37	
Ce ₂ O ₃	0.09	0.08	0.07	0.00	0.11	0.08	0.00	0.00	0.08	0.00	0.00	0.00	0.00	0.07	0.00	0.00	0.00	0.00	0.00	
Er ₂ O ₃	0.29	0.00	0.00	0.22	0.17	0.21	0.00	0.00	0.23	0.24	0.00	0.00	0.31	0.16	0.00	0.00	0.00	0.00	0.00	
Yb ₂ O ₃	0.00	0.00	0.17	0.18	0.18	0.19	0.23	0.00	0.20	0.18	0.00	0.00	0.22	0.24	0.00	0.00	0.00	0.00	0.00	
total	99.35	99.62	99.22	98.94	99.19	98.93	99.60	98.55	98.75	98.25	98.34	100.16	100.07	99.68	99.87	100.55	99.77	99.38	99.94	
ZrO ₂ /HfO ₂	72.61	79.80	78.36	74.41	72.45	75.98	76.70	82.44	87.02	71.75	77.55	89.96	82.59	84.10	69.48	79.31	74.91	78.56	78.56	
ΣREE	1.38	0.69	0.88	1.33	1.37	1.55	0.72	0.56	1.46	1.16	0.61	0.39	1.19	1.33	0.46	0.05	0.42	0.25	0.37	
P	0.000	0.000	0.000	0.000	0.000	0.000	0.002	0.000	0.001	0.001	0.000	0.000	0.001	0.000	0.000	0.000	0.001	0.000	0.000	
Si	0.987	0.991	0.987	0.988	0.991	0.993	0.987	0.994	0.990	0.993	0.993	0.986	0.982	0.988	0.989	0.983	0.988	0.990	0.986	
Σ B	0.987	0.991	0.987	0.988	0.991	0.993	0.989	0.994	0.991	0.994	0.993	0.986	0.984	0.988	0.989	0.983	0.989	0.990	0.986	
Ti	0.002	0.000	0.000	0.000	0.000	0.000	0.000	0.000	0.000	0.000	0.000	0.000	0.000	0.000	0.000	0.002	0.000	0.000	0.000	
Zr	0.987	0.992	0.995	0.988	0.985	0.982	0.995	0.991	0.985	0.984	0.990	1.002	0.997	0.989	0.997	1.006	0.998	1.000	1.002	
Hf	0.008	0.007	0.007	0.008	0.008	0.008	0.008	0.007	0.007	0.008	0.007	0.007	0.007	0.007	0.008	0.009	0.007	0.008	0.007	
Th	0.001	0.001	0.001	0.001	0.001	0.001	0.000	0.002	0.001	0.001	0.002	0.001	0.000	0.002	0.000	0.000	0.000	0.000	0.000	
Y	0.017	0.010	0.011	0.015	0.015	0.018	0.008	0.009	0.016	0.012	0.010	0.006	0.011	0.014	0.007	0.001	0.007	0.004	0.006	
Ce	0.001	0.001	0.001	0.000	0.001	0.001	0.000	0.000	0.001	0.000	0.000	0.000	0.003	0.001	0.000	0.000	0.000	0.000	0.000	
Er	0.003	0.000	0.000	0.002	0.002	0.002	0.000	0.002	0.002	0.002	0.000	0.000	0.003	0.002	0.000	0.000	0.000	0.000	0.000	
Yb	0.000	0.000	0.002	0.002	0.002	0.002	0.002	0.000	0.002	0.002	0.000	0.000	0.002	0.002	0.000	0.000	0.000	0.000	0.000	
Σ A	1.018	1.011	1.017	1.016	1.014	1.013	1.013	1.009	1.014	1.010	1.009	1.016	1.020	1.017	1.013	1.017	1.012	1.012	1.015	
Σ REE	0.020	0.011	0.013	0.019	0.020	0.023	0.010	0.009	0.021	0.016	0.010	0.006	0.016	0.019	0.007	0.001	0.007	0.004	0.006	

Table 3. Electron microprobe analyses of zircon from the Mariupol massif

ZIRCON FROM MARIUPOLITE IN SE UKRAINE

(ii) are also relatively poor in Th (0.000–0.002 apfu, 0.00–0.34 wt.% ThO₂). The sum of REEs varies in range from 0.000 to 0.019 apfu (0.00–1.33 wt.% REE₂O₃). The content of P is lower, i.e. up to 0.001

apfu, 0.00–0.05 wt.% P₂O₅. The hafnium content is up to 0.009 apfu, 0.72–1.04 wt.% HfO₂. The analytical totals are high, i.e. 98.18–100.55 wt.%. The ZrO₂/HfO₂ ratios vary from 65 to 92. Finally, the

crystal region	bright patches													dark patches						
	3	14	15	19	22	23	29	32	34	35	40	1	5	8	9	11	12	13	16	
P ₂ O ₅	0.00	0.00	0.00	0.00	0.00	0.00	0.07	0.00	0.05	0.05	0.00	0.00	0.05	0.00	0.00	0.00	0.05	0.00	0.00	
SiO ₂	31.73	32.09	31.73	31.66	31.83	31.81	31.92	31.85	31.68	31.64	31.75	32.07	31.81	31.88	32.09	32.09	32.07	31.98	32.03	
TiO ₂	0.07	0.00	0.00	0.00	0.00	0.00	0.00	0.00	0.00	0.00	0.00	0.00	0.00	0.00	0.00	0.07	0.00	0.00	0.00	
ZrO ₂	65.08	65.88	65.61	64.93	64.93	64.51	66.03	65.13	64.65	64.31	64.93	66.84	66.23	65.46	66.36	67.31	66.40	66.26	66.70	
HfO ₂	0.90	0.83	0.84	0.87	0.90	0.85	0.86	0.79	0.74	0.90	0.84	0.74	0.80	0.78	0.96	1.04	0.84	0.88	0.85	
ThO ₂	0.19	0.14	0.17	0.15	0.16	0.20	0.00	0.22	0.17	0.19	0.22	0.11	0.00	0.24	0.00	0.00	0.00	0.00	0.00	
Y ₂ O ₃	1.00	0.61	0.63	0.93	0.91	1.07	0.50	0.56	0.94	0.74	0.61	0.39	0.66	0.86	0.46	0.05	0.42	0.25	0.37	
Ce ₂ O ₃	0.09	0.08	0.07	0.00	0.11	0.08	0.00	0.00	0.08	0.00	0.00	0.00	0.00	0.07	0.00	0.00	0.00	0.00	0.00	
Er ₂ O ₃	0.29	0.00	0.00	0.22	0.17	0.21	0.00	0.00	0.23	0.24	0.00	0.00	0.31	0.16	0.00	0.00	0.00	0.00	0.00	
Yb ₂ O ₃	0.00	0.00	0.17	0.18	0.18	0.19	0.23	0.00	0.20	0.18	0.00	0.00	0.22	0.24	0.00	0.00	0.00	0.00	0.00	
total	99.35	99.62	99.22	98.94	99.19	98.93	99.60	98.55	98.75	98.25	98.34	100.16	100.07	99.68	99.87	100.55	99.77	99.38	99.94	
ZrO ₂ /HfO ₂	72.61	79.80	78.36	74.41	72.45	75.98	76.70	82.44	87.02	71.75	77.55	89.96	82.59	84.10	69.48	64.86	79.31	74.91	78.56	
ΣREE	1.38	0.69	0.88	1.33	1.37	1.55	0.72	0.56	1.46	1.16	0.61	0.39	1.19	1.33	0.46	0.05	0.42	0.25	0.37	
P	0.000	0.000	0.000	0.000	0.000	0.000	0.002	0.000	0.001	0.001	0.000	0.000	0.001	0.000	0.000	0.000	0.001	0.000	0.000	
Si	0.987	0.991	0.987	0.988	0.991	0.993	0.987	0.994	0.990	0.993	0.993	0.986	0.982	0.988	0.989	0.983	0.988	0.990	0.986	
Σ B	0.987	0.991	0.987	0.988	0.991	0.993	0.989	0.994	0.991	0.994	0.993	0.986	0.984	0.988	0.989	0.983	0.989	0.990	0.986	
Ti	0.002	0.000	0.000	0.000	0.000	0.000	0.000	0.000	0.000	0.000	0.000	0.000	0.000	0.000	0.000	0.002	0.000	0.000	0.000	
Zr	0.987	0.992	0.995	0.988	0.985	0.982	0.995	0.991	0.985	0.984	0.990	1.002	0.997	0.989	0.997	1.006	0.998	1.000	1.002	
Hf	0.008	0.007	0.007	0.008	0.008	0.008	0.008	0.007	0.007	0.008	0.007	0.007	0.007	0.007	0.008	0.009	0.007	0.008	0.007	
Th	0.001	0.001	0.001	0.001	0.001	0.001	0.000	0.002	0.001	0.001	0.002	0.001	0.000	0.002	0.000	0.000	0.000	0.000	0.000	
Y	0.017	0.010	0.011	0.015	0.015	0.018	0.008	0.009	0.016	0.012	0.010	0.006	0.011	0.014	0.007	0.001	0.007	0.004	0.006	
Ce	0.001	0.001	0.001	0.000	0.001	0.001	0.000	0.000	0.001	0.000	0.000	0.000	0.000	0.001	0.000	0.000	0.000	0.000	0.000	
Er	0.003	0.000	0.000	0.002	0.002	0.002	0.000	0.000	0.002	0.002	0.000	0.000	0.003	0.002	0.000	0.000	0.000	0.000	0.000	
Yb	0.000	0.000	0.002	0.002	0.002	0.002	0.002	0.000	0.002	0.002	0.000	0.000	0.002	0.002	0.000	0.000	0.000	0.000	0.000	
Σ A	1.018	1.011	1.017	1.016	1.014	1.013	1.013	1.009	1.014	1.010	1.009	1.016	1.020	1.017	1.013	1.017	1.012	1.012	1.015	
Σ REE	0.020	0.011	0.013	0.019	0.020	0.023	0.010	0.009	0.021	0.016	0.010	0.006	0.016	0.019	0.007	0.001	0.007	0.004	0.006	

Table 3. Electron microprobe analyses of zircon from the Mariupol massif c. d.

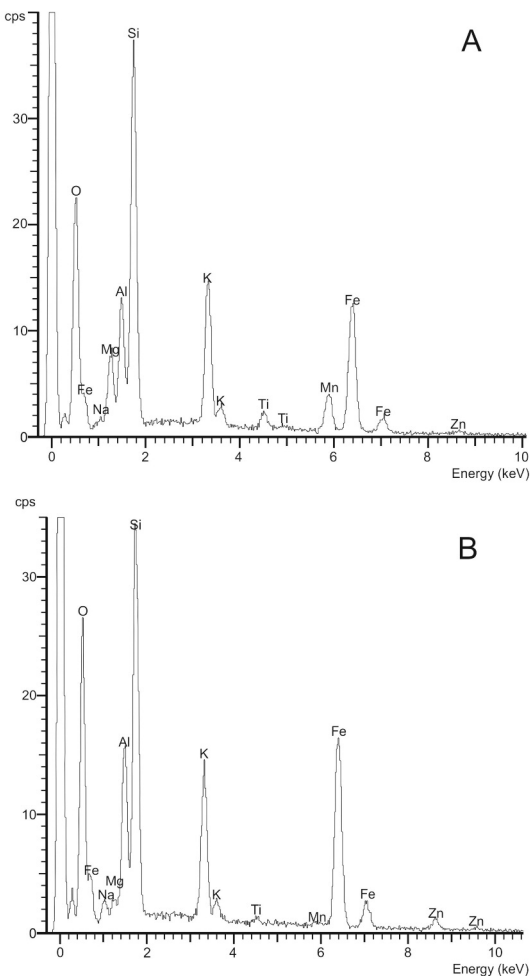
darkest patches (iii) are almost completely devoid of REEs (0.00–0.01 wt.% REE₂O₃). The contents of P and Th are under their detection limit. The hafnium concentration is elevated (0.007–0.010 apfu, 0.77–1.11 wt.% HfO₂). The analytical totals are high, i.e. 98.18–100.83 wt.%. The ZrO₂/HfO₂ ratios vary from 61 to 88.

Most of the zircon crystals show irregular domains where the cathodoluminescence is yellow with slight variations in its intensity (Text-fig. 8). Among these, dark areas with dark green/navy blue CL are observed within the crystals. Similarly to the BSE observations (Text-fig. 3), CL imaging also revealed oscillatory zoning along the edges of the crystals with navy blue CL. The dark areas in BSE are bright in CL and vice versa.

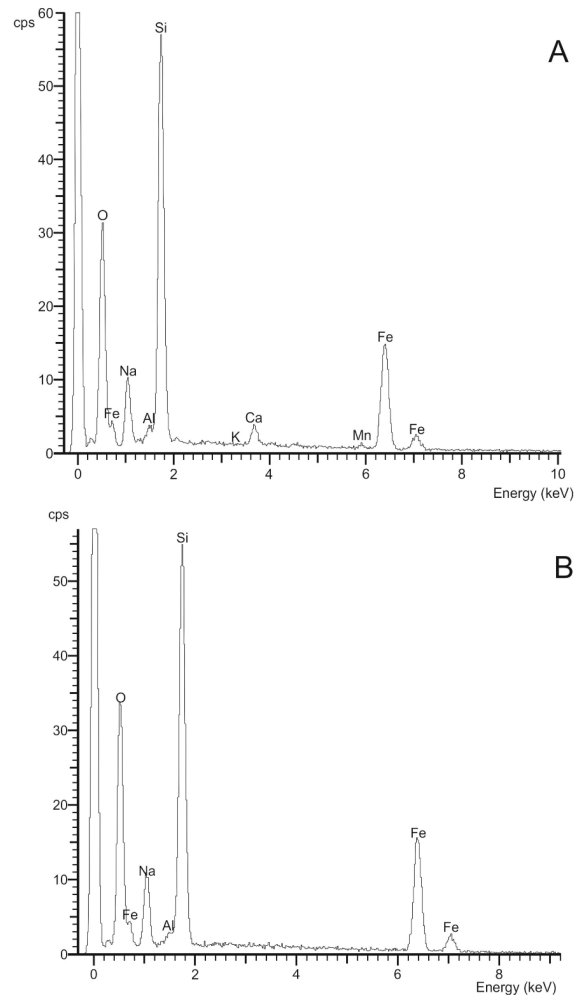
CL emission spectra were recorded for the domains with both yellow CL and navy blue CL, with some variations in the intensity. The spectra obtained for the yellow CL domains (the darkest regions in BSE) are

nearly identical. The domains with green CL (dark in BSE) and dark green/navy blue CL (bright in BSE) produce emission spectra with varying luminescence intensity. The yellow CL domains are characterized by an intense emission line at 555 nm activated most likely by Yb²⁺ (Text-fig. 9). The presence of Yb²⁺ in the zircon structure is a result of the radioactive interaction of U (and Th) with Yb³⁺ (Nasdala *et al.* 2003). The line at 390 nm is due to intrinsic defects in the [SiO₄] groups. The region of the crystals with dark green CL produce spectra (Text-fig. 10) with distinct emission lines at 480 and 575 nm attributed to Dy³⁺ activation (Zr⁴⁺ is substituted for Dy³⁺) (Gorobets and Rogojine 2002). A far less intense peak near 390 nm is also observed in these spectra. The emission lines arising from radiation-induced centres and from Dy³⁺ obscure the spectra of other REE elements, as a consequence of which the weaker emission lines are difficult to interpret.

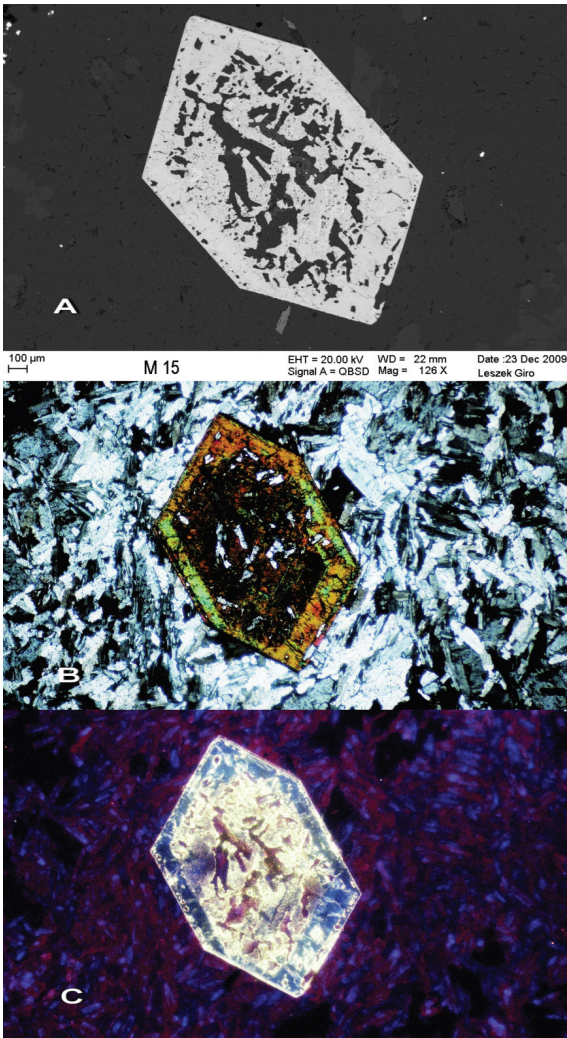
The significant differences in both types of CL spec-



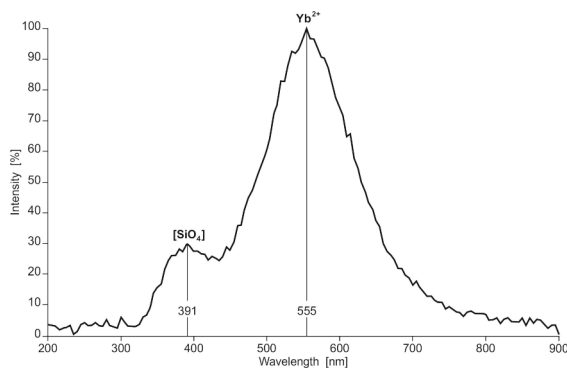
Text-fig. 6. EDS spectra of lepidomelane in the host rock matrix (A) and zircon crystal (B)



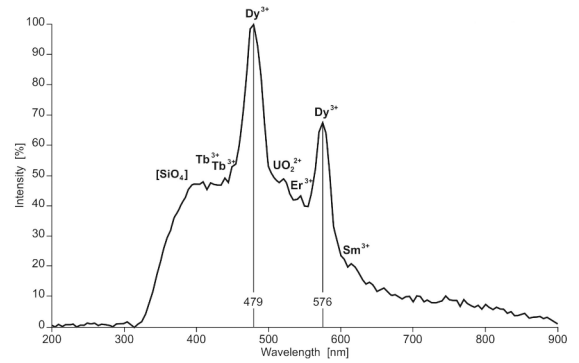
Text-fig. 7. EDS spectra of aegirine in the host rock matrix (A) and zircon crystal (B)



Text-fig. 8. Zircon crystal in a feldspar matrix. A – Numerous inclusions in the interior of zircon. Light margins of the crystal (dark in CL) distinctly impoverished in the inclusions (BSE image); B – Inclusions of feldspars in zircon (polarized light, crossed polarizers); C – Note the navy blue CL of the crystal margin and the yellow CL in the interior of the zircon. The feldspar matrix shows pink and violet-pink CL colours due to the fenitization process (CL image)



Text-fig. 9. A CL emission spectrum of the navy blue-luminescing margin of a zircon crystal



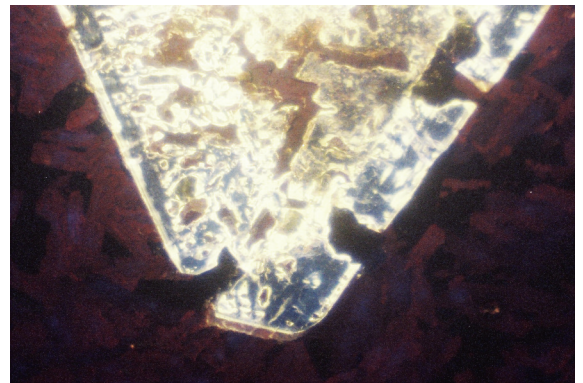
Text-fig. 10. A CL emission spectrum of the yellow-luminescing interior of a zircon crystal

tra indicate that the domains with yellow CL differ in origin from the areas of crystals with dark green CL.

DISCUSSION

The areas with abundant micropores filled with numerous inclusions such as albite, K-feldspar, lepidomelane, aegirine, pyrochlore and REE-bearing carbonates correspond to the patchy zoning in the zircon interiors. The outer parts of the crystals with characteristic oscillatory zoning, and considerably impoverished in inclusions, are the least fractured regions of the zircons and are almost free of micropores. Hence it seems that zircon corrosion affected mostly the central, most fractured part of the crystals. During its leaching some irregular corrosion pits (micropores), mostly rounded in shape, formed (Text-fig. 11).

Mariupolite obviously includes different generations of mineral phases. Undoubtedly, the crystallization of the mineral associations of the host rock took place in stages. Aegirine, nepheline, lepidomelane and zircon form megacrystals within a medium-crystalline albite matrix. The short and thin tabular crystals of albite surround these megacrystals and clearly adjust to



Text-fig. 11. A region of zircon crystal with corrosion embayments filled with albite (CL image)

their shape. In the vicinity of zircon the majority of albite crystals are elongated parallel to the (100), (110) or (010) faces of the zircon crystals. Albite shows atypical pink and violet-pink CL colours, thereby indicating that it was altered by the fenitization process (Mariano 1978; Marshall 1988). Hence, in the first stage of the aluminosilicate magma differentiation process aegirine, nepheline, lepidomelane and finally zircon crystallized. The crystallization of the zircon was most probably contemporaneous with the formation of its inclusions, i.e. aegirine and lepidomelane. However, the differences in the composition of these minerals occurring in both the host rock matrix and zircon crystals suggest that the inclusions definitely crystallized at a lower temperature than the megacrystals forming the mariupolite matrix. During the crystallization of the megacrystals the formation of albite – the main component of the host rock – was initiated. Then, in the next stage, some minerals underwent alteration through the influence of a strong alkaline medium, i.e., the zircon was affected by corrosion; natrolitization of primary nepheline and chloritization of lepidomelane took place. Hence, the zircon inclusions such as aegirine, lepidomelane, albite and K-feldspar and pyrochlore were probably enclosed by faster growing zircon crystal. Other zircon inclusions, i.e. paristite and bastnäsite-(Ce) are certainly secondary phases.

The patchy zoning texture of zircon from *mariupolite* indicates that its formation occurred over a long period of time and under various temperature conditions. Tomaschek *et al.* (2003) and Xie *et al.* (2005) attributed such a texture to fluid interaction with zircon. It is likely that in a post-magmatic setting low temperatures and hydrothermal processes could have produced the pores in zircon. However, the hydrothermal process would be expected to operate at the low temperature post-magmatic stage, while the vast majority of the pores occur mainly in the internal parts of crystals. Moreover the porous parts of zircon are surrounded by oscillatory zoning, which is characteristic of the magmatic stage (Hoskin and Schaltegger 1993). The hydrothermal alteration of zircon is also associated with an enrichment in Fe and Ca (Geisler and Schlicher 2000), whereas the patchy regions contain very low amounts of Fe, similarly to the unaltered parts of grains. Gagnevin *et al.* (2009) suggested that such a patchy zoning texture could be ascribed to certain disequilibrium processes that occur during zircon growth in a high-temperature environment $> 700^{\circ}\text{C}$. Geisler *et al.* (2007) attributed the origin of this texture to a dissolution-recrystallization process. Kempe *et al.* (2000) concluded that thermal recrystallization takes place in defect-rich domains in crystals, such as metamict cores,

defect-rich sectors in sector zoning and boundaries between growth zones in oscillatory zoning.

The slightly variable chemical composition of the zircon, in particular the REE and Th content, also indicates that its formation took place in variable geochemical environments. Besides irregular domains rich in REE_2O_3 (average 1.06 wt.%) and ThO_2 (average 0.16 wt.% – light patches in BSE), there are other domains that are almost completely depleted in these trace elements. The darkest patches of zircon are almost devoid of REE_2O_3 and ThO_2 . Hence, this is a typical disequilibrium texture manifested by the replacement of Th-REE – rich zircon by Th-REE-poor zircon together with abundant micropores and various mineral inclusions (Gagnevin *et al.* 2009). The regions depleted in REEs with yellow CL are most probably thermally recrystallized regions of zircon (Nasdala *et al.* 2003). They are characterized by a higher degree of crystallinity (a distinct emission line at 396 nm attributed to a perfect crystal lattice observed in CL spectra) probably resulting from the impoverishment of the zircon structure in REEs or from the regeneration of structural defects caused by the influence of radioactive elements. The former hypothesis seems to be more probable in this case. In CL spectra taken from CL bright (darkest in BSE) domains there are distinctly fewer peaks due to the presence of REEs (Dy^{3+} , Yb^{2+}) than in those recorded for CL dark (bright in BSE) regions (Dy^{3+} , Tb^{3+} , Er^{3+} , Sm^{3+} (?), UO_2^{2+}). The recrystallization of the yellow CL regions was caused by the relative instability of the domains rich in trace elements compared with the zircon crystals depleted in these elements (Corfu *et al.* 2003). In this process, the trace elements are removed from the structure and the zircon exhibits a simple, monotonous chemical composition. It is very probable that the REEs removed from the zircon were later incorporated into the structure of REE-bearing carbonates (paristite, bastnäsite-(Ce)) appearing as inclusions in the zircon. As was explained by Geisler *et al.* (2007), the decrease in trace elements (here REEs, Th) and the occurrence of micropores and inclusions at the recrystallization front were due to the fact that the zircon solid solution (i.e., zircon rich in trace elements) has a higher solubility than pure zircon. It follows that zircon formed by dissolution and then recrystallization will be poorer in trace elements than zircon in its original form (Rubatto *et al.* 2008).

To sum up, both chemical and textural observations of zircon taken from the Mariupol Massif lead to the conclusion that typical magmatic zircon from *mariupolite* with oscillatory zoning was strongly influenced by dissolution and recrystallization processes during the late magmatic or post-magmatic stage of host rock cooling.

Acknowledgements

The contributions from Adam Pieczka for his valuable suggestions and discussion during the preparation of the manuscript, as well as from Leszek Giro for performing BSE and SEM-CL analyses, are gratefully acknowledged. We sincerely thank the reviewers, Jaromir Leichmann and Bartosz Budzyń for their friendly comments and careful revision on the final version of the manuscript. Special thanks go to Ewa Słaby for her helpful remarks during preparation of this paper. Thanks are also to Chris Wood for language revision of the manuscript. The work was financially supported by the AGH – University of Science and Technology (Krakow, Poland), the research project no 11.11.140.158.

REFERENCES

- Belousova, E.A., Griffin, W.L. and Pearson, N.J. 1998. Trace element composition and cathodoluminescence properties of southern African kimberlitic zircons. *Mineralogical Magazine*, **62** (3), 355–366.
- Belousova, E.A., Griffin, W.L., O'Reilly, Suzanne Y. and Fisher, B.I. 2002. Igneous zircon: trace element composition as an indicator of source rock type. *Contributions to Mineralogy and Petrology*, **143**, 602–622.
- Corfu, F., Hanchar, J.M., Hoskin, P.W.O. and Kinny, P.D. 2003. Atlas of zircon texture. Mineralogical Society of America, *Reviews in Mineralogy and Geochemistry*, **51** (1), 469–500.
- Deer, W.A., Howie, R.A. and Zussmann, J. 1992. An introduction to the rock forming minerals, 696 pp. Pearson Education Limited; Essex. [2nd Edition]
- Donskoy, A.N. 1982. The nepheline complex of alkaline Oktyabr'skii massif, 150 pp. The Ukrainian Academy of Science; Kiev. [In Ukrainian]
- Dumańska-Słowik M., Baranov P., Heflik W., Natkaniec-Nowak L., Shevchenko S., Tsotsko L.I. 2011. Mariupolite from the Oktyabrsky Massif (SE Ukraine) – a less known rock in the gemstone trade, *Zeitschrift der Deutschen Gemmologischen Gesellschaft* **60** (1-2), 37–48.
- Gaft, M., Reisfeld, R. and Panczer, G. 2005. Luminescence Spectroscopy of Minerals and Materials, 356 pp. Springer-Verlag Berlin; Heidelberg.
- Gagnevin, D., Daly, J.S. and Kronz, A. 2009. Zircon texture and chemical composition as a guide to magmatic process and mixing in a granitic environment and coeval volcanic system. *Contributions to Mineralogy and Petrology*, **159** (4), 579–596.
- Geisler, T. and Schleicher, H. 2000. Improved U-Th total Pb dating of zircons by electron microprobe using a simple new background modelling procedure and Ca as a chemical criterion of fluid-induced U-Th-Pb discordance in zircon. *Chemical Geology*, **163**, 269–285.
- Geisler, T., Rashwan, A.A., Rahn, M.K., Poller, U., Zwingmann, H., Pidgeon, R.T., Schleicher, H. and Tomaschenk, F. 2003. Low-temperature hydrothermal alteration of natural metamict zircons from the Eastern Desert, Egypt. *Mineralogical Magazine* **67** (3), 485–508.
- Geisler, T., Schaltegger, U. and Tomaschek, F. 2007. Re-equilibration of zircon in aqueous fluids and melts. *Elements*, **3** (1), 43–50.
- Gorobets, B.S. and Rogojine, A.A. 2002. Luminescent spectra of minerals, 300 pp. Moscow.
- Götze, J. 2000. Cathodoluminescence microscopy and spectroscopy in applied mineralogy, pp. 1–128. Geowissenschaften C 485. Tech. Univ. Bergakad. Freiberg.
- Hanchar, J.M. and Miller, C.F. 1993. Zircon zonation patterns as revealed by cathodoluminescence and backscattered electron images: Implication for interpretation of complex crustal histories. *Chemical Geology*, **110**, 1–13.
- Hinton, R.W. and Upton, B.G.J. 1991. The chemistry of zircon: Variation within and between large crystals from syenite and alkali basalt xenoliths. *Geochimica et Cosmochimica Acta*, **55**, 3287–3302.
- Hoskin, P.W.O. 2005. Trace-element composition of hydrothermal zircons and the alteration of Hadean zircon from the Jack Hills, Australia. *Geochimica et Cosmochimica Acta*, **69** (3), 637–648.
- Hoskin, P.W.O. and Schaltegger, U. 1993. The composition of zircon and igneous and metamorphic petrogenesis. *Reviews in Mineralogy and Geochemistry*, **53**, 27–62.
- Kempe, U., Gruner, T., Nasdala, L.I. and Wolf, D. 2000. Relevance of cathodoluminescence for the interpretation of U–Pb zircon ages, with an example of an application to a study of zircons from the Saxonian Granulite Complex, Germany. In: M. Pagel, V. Barbin, P. Blanc, D. Ohnenstetter (Eds), *Cathodoluminescence in Geosciences*, pp. 425–456.
- Krivdik, S.G. and Tkachuk, V.I. 1988. Geochemical and petrological characterization of the rocks from the alkaline Oktyabr'skii Massif (Ukraine). *Geochimija*, **4**, 362–371. [In Russian]
- Krivdik, S.G., Nivin, V.A., Kul'chitskaya, A.A., Voznak, D.K., Kalinichenko, A.M., Zagnitko, V.N. and Dubyna, A.V. 2007. Hydrocarbons and other volatile components in alkaline rocks from the Ukrainian Shield and Kola Peninsula. *Geochemistry International*, **45** (3), 270–294.
- Mariano, A.N. 1978. The application of cathodoluminescence for carbonatite exploration and characterization. In: C.J. Braga (Ed.), *Proceedings of the International Symposium on Carbonatites*, pp. 39–57.
- Marshall, D.J. 1988. Cathodoluminescence of Geological Materials. Unwin Hyman, p. 146.
- Morozewicz, J. 1902. Über Mariupolit, ein extremes Glied der Elaeolithsyenite. *Tschermaks Mineralogische und Petrographische Mitteilungen*, **21**, 238–246.

- Morozewicz, J. 1929. Mariupolite and its relatives. *Prace Polskiego Instytutu Geologicznego* **2** (3), p. 130. [In Polish]
- Murali, A.V., Parthasarathy, T.M., Mahadevan, T.M. and Sankar, Das M. 1983. Trace element characteristics, REE patterns and partition coefficients of zircons from different geological environments – A case study on Indian zircons. *Geochimica et Cosmochimica Acta*, **47**, 2047–2052.
- Nasdala, L., Zhang, M., Kempe, U., Panczer, G., Gaft, M., Andrut, M. and Plötze, M. 2003. Spectroscopic methods applied to zircon. In: Hanchar J. and Hoskin P. (Eds), *Zircon, Reviews in Mineralogy and Geochemistry*, **53**, 427–466.
- Pouchou, I.L. and Pichoir, F. 1985. “PAP” (phi-rho-z) procedure for improved quantitative microanalysis. In: I.T. Armstrong (Ed.), *Microbeam Analysis*, pp. 104–106. San Francisco Press; San Francisco.
- Rubatto, D. and Gebauer, D. 2000. Use of cathodoluminescence for U-Pb zircon dating by ion microprobe: some examples from the Western Alps. In: M. Pagel, V. Barbin, P. Blanc, D. Ohnenstetter (Eds), *Cathodoluminescence in Geosciences*, Springer, Berlin–Heidelberg 373–400.
- Rubatto, D., Müntener, O., Barnhoorn, A. and Gregory, C. 2008. Dissolution-precipitation of zircon at low-temperature, high-pressure conditions (Lanzo Massif, Italy). *American Mineralogist*, **93**, 1519–1529.
- Rubin, J.N., Henry, C.D. and Price, J.G. 1989. Hydrothermal zircons and zircon growths, Sierra Blanca Peaks, Texas. *American Mineralogist*, **74**, 865–869.
- Sharygin, V.V., Krivdik, S.G., Pospelova, L.N. and Dubina A.V. 2009. Zn-kupletskite and hendricksite in the agpaitic phonolites of the Oktyabrskii Massif, Azov region, Ukraine. *Doklady Earth Sciences*, **425** (3), 499–504.
- Solodov, N.A. 1985. The mineralo-genesis of rare metal formations, 225 pp. Nedra. Moscow. [In Ukrainian]
- Tichonienkova, R.J., Osokin, J.D., Gonzejev, A.A. 1967. Rare-metals metasomatites of alkaline massives, Nauka, Moscow, 196 pp. [In Ukrainian]
- Tomaschek, F., Kennedy, A.K., Villa, I.M., Lagos, M. and Ballhaus, C. 2003. Zircon from Syros, Cyclades, Greece – recrystallization and mobilization of zircon during high-pressure metamorphism. *Journal of Petrology*, **44** (11), 1977–2002.
- Vavra, G., Schmid, R. and Gabauer, D. 1999. Internal morphology, habit and U-Pb microanalysis of amphibolite-to-granulite facies zircons: geochronology of the Ivrea Zone (Southern Alps). *Contributions to Mineralogy and Petrology*, **134**, 380–404.
- Volkova, T.P. 2000. The genesis and ore mineralization of alkaline rocks from the Oktyabr'skii Massif. *Sbornik nauchnykh trudov*, **4**, 9–10. [In Ukrainian]
- Volkova, T.P. 2001. The productivity criterion of REE and ore mineralization within rocks of the Oktyabr'skii Massif. *Naukovi praci DonDTU*, **36**, 63–69. [In Ukrainian]
- Xie, L., Wang, R., Chen, X., Qiu, J. And Wang, D. 2005. Th-rich zircon from peralkaline A-type granite: mineralogical features and petrological implications. *Chinese Science Bulletin*, **50**, 809–817.

Manuscript submitted: 10th October 2010

Revised version accepted: 15th April 2011